CHAPTER NINE

Electron Density Plot Calculations and Display

9.1 Introduction

The *DC* program calculates electron density plots for a solid or a layered structure on a cross-section plane that is parallel to the ab-, ac- or bc-plane of its unit cell. Partial electron density plots are obtained by using the energy levels belonging to a certain narrow energy region, while total electron density plots by using all the occupied energy levels. The *DP* program displays electron density plots calculated by the *DC* program. For a layered structure designed to simulate a solid surface, partial and total electron density plots of interest are "surface density plots" (SDP) calculated on cross-section planes that are parallel to and lie above the surface at a certain distance.

Atomic- and molecular-scale STM and AFM images are almost routinely recorded for crystalline surfaces, but the interpretation of these images is not necessarily straightforward because the tip-sample force interaction may induce a surface corrugation, which depends on the variation of the local stiffness of the sample surface. If the tip-force induced surface corrugation is neglected, an STM image of a sample surface recorded with positive bias voltage is described by a partial SDP associated with the lowest unoccupied energy levels of the sample surface, and an STM image recorded with negative bias voltage by a partial SDP associated with the highest occupied energy levels. An AFM image of a sample surface is described by the total SDP resulting from all the occupied energy levels of the sample surface.[1]

The *DC* program of the *CAESAR* package calculates the partial and total electron density plots of a solid or a layered structure, while the *DP* program displays these density plots.

9.2 Electron density calculation program *DC*

The simplest and most practical theory of STM was developed by Tersoff and Hamman.[2] The three crucial assumptions of this theory are (1) the tip can be approximated by an atom with an s-orbital, (2) the tip-sample force interaction is negligible, and (3) the bias voltage is small. Assumptions (1), (2) and (3) respectively allow one to treat the tip as a mathematical point, to neglect possible modifications of the structures and wave functions of both electrodes, and to consider only the electronic states of the sample near the Fermi level for the tunneling process. Under these assumptions, the STM current is proportional to the local density of states of the sample at the position of the tip above the sample surface. Then the equi-current contours observed in constant-height STM measurements correspond to the constant contours of the partial SDP $\rho(r_0, e_f)$ of the sample surface around the Fermi level, evaluated at the tip-to-sample distance r_0. Therefore, for a given sample surface, the brightness pattern of the STM image is related to the high-density pattern of the $\rho(r_0, e_f)$ plot.

The force between closed-shell atoms and molecules are primarily determined by the outer regions of the atoms, in which the atomic electron densities overlap. Therefore, if AFM tip is approximated by an atom and if the surface topography is negligibly affected by the tip-sample interactions, it is expected that the repulsive force experienced by the tip in contract-model AFM is proportional to the total electron density of the sample at the position of the tip r_0 from the sample surface. Thus, the equi-force contours in constant-height AFM measurements correspond to constant contours of the total electron density plot $\rho(r_0)$ of the sample surface at the position of the tip-to-sample distance r_0.[1] Therefore, for a given sample surface, the brightness pattern of the AFM image is related to the high-density pattern of the $\rho(r_0)$ plot.

9.2.1 STM image simulation

When the geometry of a sample is known, it is straightforward to calculate the $\rho(r_0, e_f)$ plots from its electronic structure. For a layered materials, the surface reconstruction is negligible so that the geometry of the surface layer is well approximated by the layer geometry of the bulk crystal structure. In general, the contribution of an atom to the $\rho(r_0, e_f)$ plot increases as its distance to the tip decreases and as its electronic contribution to the energy levels around the Fermi level increases. Since the more-protruding atoms do not necessarily make more contributions to the energy levels near the Fermi level, it is difficult to interpret STM images unless appropriate partial density plots are calculated.

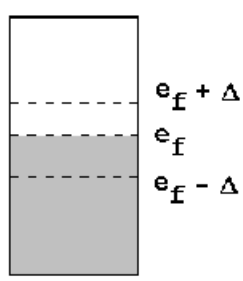

Figure 9.1. Energy windows appropriate for the partial density plot calculations of a metal.

The *DC* program takes three steps to make the $\rho(r_0, e_f)$ plot: (1) Calculate the band orbitals $\psi_i(k)$ and band orbital energies $e_i(k)$ of a sample surface for a set of k-points sampling the whole FPZ. (2) Select the band levels appropriate for the partial electron density calculation. They lie between e_f and $e_f - \Delta$ for negative bias STM images, and between e_f and $e_f + \Delta$ for positive bias STM images. Here Δ is the energy window. e_f refers to the highest occupied level for negative bias STM images, and to the lowest unoccupied level for positive bias STM images. (3) Calculate $\rho(r_0, e_f)$ at the tip-to-sample distance r_0 based on the band orbitals belong to the selected energy window.

To determine the energy range for selecting the band levels, it is necessary to run the *BC* and *PC* programs and find the Fermi level e_f. The energy window Δ is a small positive number. When the energy bands associated with tunneling are several electron volts wide, the energy window Δ can be chosen to be about 0.25 eV. For metals, the highest occupied and lowest occupied levels are degenerate (*Figure 9.1*).

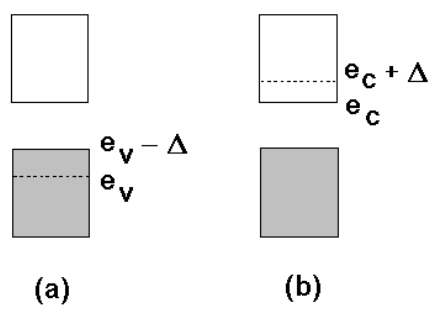

Figure 9.2. Energy windows appropriate for the partial density plot calculations for a normal semiconductor: (a) for $V_{bias} < 0$; (b) for $V_{bias} > 0$.

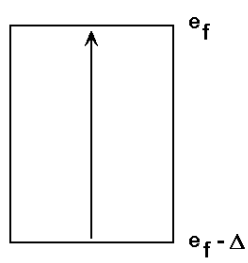

Figure 9.3. Energy windows appropriate for the partial density plot calculations for a magnetic semiconductor for both $V_{bias} < 0$ and for $V_{bias} > 0$.

The tip-to-sample distance r_0 value can be taken to be small (e.g., 0.5 Å from the atoms closest to the tip), since what matters most in interpreting images is the brightness pattern. The orbital amplitudes of the wave functions of a surface decrease exponentially with distance from the surface so

that the values of $\rho(r_0, e_f)$ become too small for meaningful comparisons if r_0 is large (e.g., 4 Å). The $\rho(r_0, e_f)$ plots calculated for r_0 = 0.5 Å have been found to reflect the essential patterns of the observed STM images rather well.[4] For the sample-to-tip tunneling of an intrinsic semiconductor, the occupied band orbitals lying between the highest occupied (i.e., valence) band level E_V and the level $E_V - \Delta$ should be selected (*Figure 9.2a*). For the tip-to-sample tunneling of an intrinsic semiconductor, the unoccupied band orbitals lying between the lowest unoccupied (e.g., conduction) band level E_C and the level $E_C + \Delta$ should be selected (*Figure 9.2b*). A magnetic semiconductor has unpaired spin orbitals responsible for its magnetic properties. The singly filled levels can either donate electrons to the tip or receive electrons from the tip. Thus, to calculate the partial density plot of a magnetic semiconductor, e_f should be set equal to the top of the partially filled band(s) and all the levels of the partially filled band(s) may be selected for both the sample-to-tip and tip-to-sample tunneling (*Figure 9.3*).

9.2.2 AFM image simulation

The total electron density plot $\rho(r_0)$ necessary for the simulation of the AFM image of a solid surface is obtained by summing up the density contributions from all the occupied band orbitals. In calculating the $\rho(r_0)$ plots, the tip-to-sample distance r_0 may be taken to be short as in the case of the $\rho(r_0, e_f)$ plot calculations for STM images.

9.2.3 Input file *filename.DI*

Before simulating STM and AFM images of a solid surface, it is necessary to understand the crystal and the electronic band structures of the solid system under examination. This can be achieved by using the *Builder*, *BC*, *PC* and *PP* programs of the *CAESAR* package.

The input file *filename.DI* for running the *DC* program can be created by employing the *NEWDI* program. When the *NEWDI* program is launched, it opens the *New .DI File* dialog box (*Figure 9.4*), which is used to create a *filename.DI* file. The *New .DI File* dialog box has a number of parameter fields to consider. The basic ones are discussed in this section.

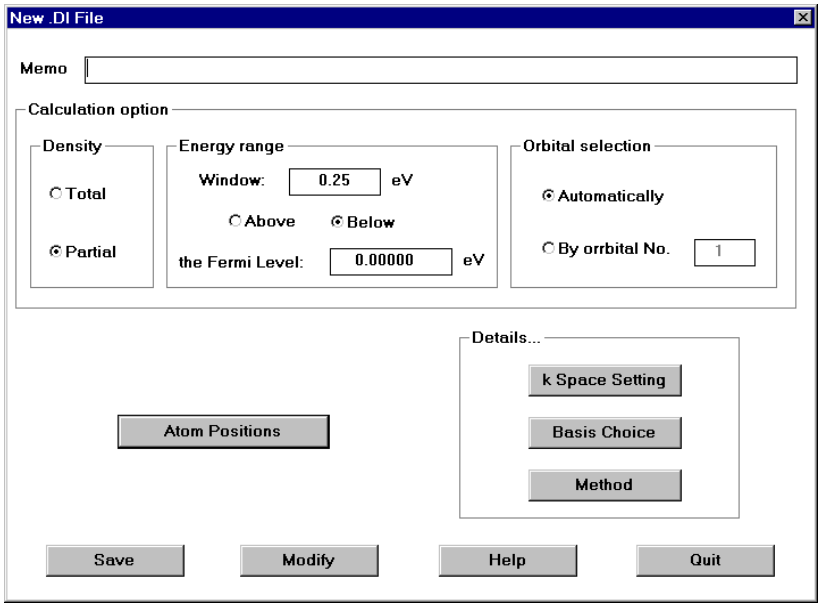

Figure 9.4. New .DI File dialog box.

• ***Memo***

This is used to add a short comment about a calculation in question.

• ***Calculation Option***

This field has three different parts to consider:

(1) In the *Density* field, one should specify whether a current calculation is for a *Total* or *Partial* electron density plot.

(2) The parameters in the *Energy range* field determine the energy region for total and partial density calculations. If the *Partial* option is selected, the user should specify the Δ value in the *Window* field. Then select the *Above* button to specify the energy region from e_f to $e_f + \Delta$, and the *Below* button to specify the energy region from e_f to $e_f - \Delta$. For STM image simulations, e_f refers to the Fermi level for a normal metal. As already mentioned, the meaning of the Fermi level for normal semiconductors and magnetic semiconductors is different from that for normal metals. (For calculating any general partial density plot, e_f can be any energy level). The Fermi level can be obtained by reviewing the output files *filename.BO* or *filename.PO*. If the *Total* option is selected, the *Above* and *Below* buttons are disabled, and the energy window (e.g., the Δ value) is set to be 30.00 eV. This means that all the occupied levels lying within 30 eV from the Fermi level will be selected for total density plot calculations.

(3) The *Orbital selection* field has two options. The *Automatically* option will sample all the band levels lying within the energy range defined in the *Energy range* field. The *By orbital No.* option allows the user to select one specific band to study within the chosen energy range.

• ***Atom Positions***

Density plot calculations for a solid or a layered structure require the specification of its crystal structure, i.e., the atoms and their positions in a unit cell as well as the repeat vectors. With *CAESAR* one can create crystal structures from crystallographic data and modify them using the program *Builder* (see Chapter 3). To create a *filename.DI* file using the *NEWDI* program, one needs a crystal structure file *filename.CI*.

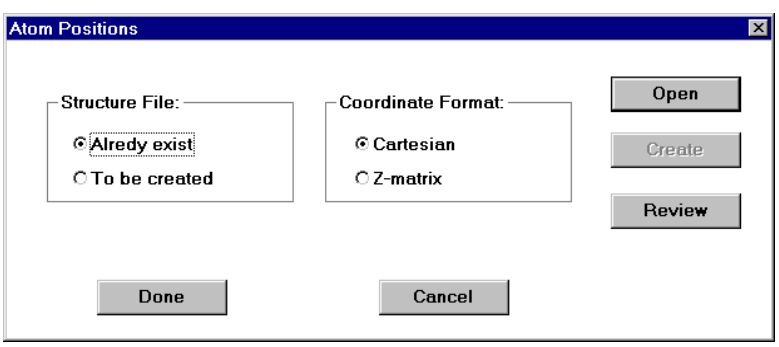

Figure 9.5. Atom Positions dialog box.

The *Atom Positions* command of the *New. DI File* box opens the *Atom Positions* dialog box (*Figure 9.5*), which has two important functions. One is to provide the coordinates of the atoms of a unit cell, and the other is to open the *Direct Space Setting* dialog box. The use of this command is described in detail in Chapter 6. After the positions of all the atoms of a unit cell are defined using the *Atom Positions* dialog box, click the *Done* button to open the *Direct Space Setting* dialog box (*Figure 9.6*). This box shows the repeat vectors defined for 2D layer under examination. The options of the drop-down list of *Vectors* provide three planes (*ab*-, *bc*- or *ac*-plane) to choose for a 2D layer.

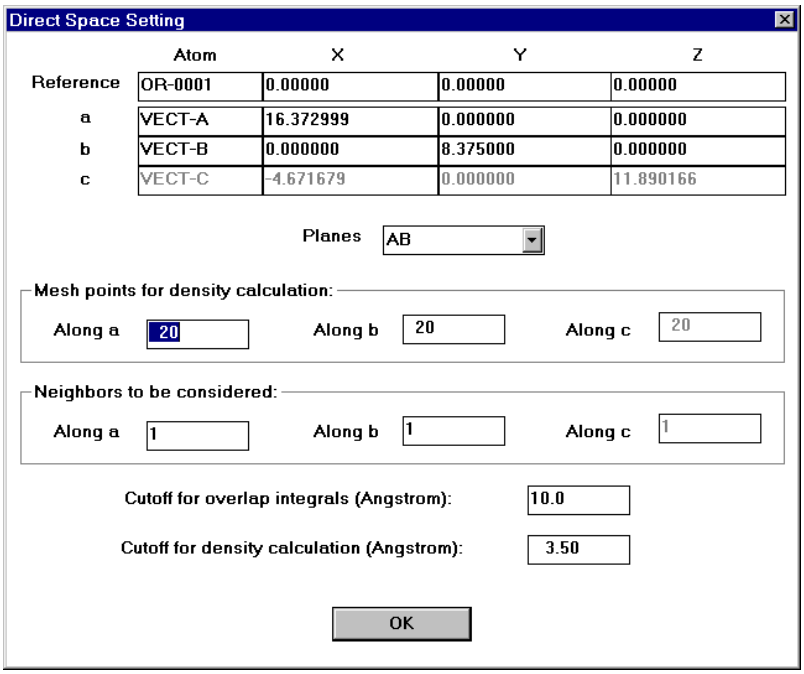

Figure 9.6. Direct Space Setting dialog box.

The mesh points specified in the *Mesh points for density calculation* field generate a set of 2D-grid points on the surface unit cell, at which the values of the surface electron density are calculated. The *Neighbors to be considered* field determines how many nearest neighbor unit cells, *n*, to include in the lattice sums. The *Cutoff for density calculation*, which has the default value of 3.5 Å, simplifies electron density calculations: For any point of the grid plane, the contribution to the electron density from an atom located beyond the *Cutoff* distance from that point is ignored. The meaning of the *Cutoff for overlap integrals* is the same as that described in Chapter 5.

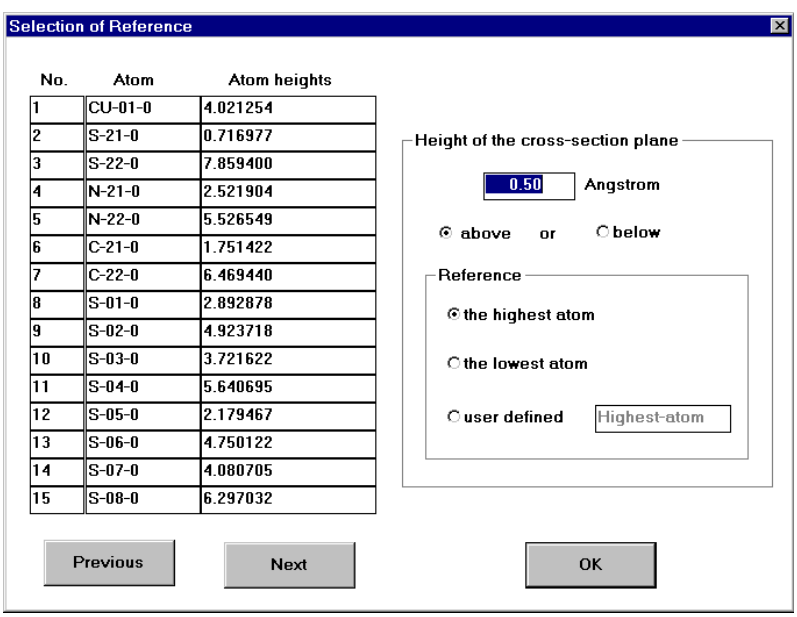

Figure 9.7. Selection of Reference dialog box.

The *OK* button of *Direct Space Setting* dialog box opens the *Selection of Reference* dialog box (*Figure 9.7*), which lists the heights of all the unit cell atoms on the left hand side. It should be noted that the cross-section plane for plotting is made parallel to the coordinate xy-plane, so that the heights of the atoms refer to their z-coordinates. The height of the cross-section plane is specified relative to the height of a reference atom. The reference atom should be one of the unit cell atoms. As is clear from the *Height of the cross-section plane* field on the right hand side, the reference atom can be the lowest-lying, the highest-lying, or any other atom the user selects.

The *Details* field of the *New .DI File* dialog box has three command buttons by which to set parameters. All these parameters should be set only after specifying the positions of atoms in the input file *filename.DI*. The use of these commands is explained in detail in Chapters 5 and 6.

9.2.4 Editing an input file *filename.DI*

The user may generate a new *filename.DI* file by editing an existing *filename.DI*. This can be achieved by using any text editor or by using the *Modify* command of the *New .DI* dialog box. When clicked, it opens the *Open* dialog box to allow the user to locate the existing file and copy its contents into the parameter fields of *New .DI File* dialog box (*Figure 9.8*). Then the user can edit the file by going through the appropriate fields of the *New .DI File* dialog box where changes have to be made.

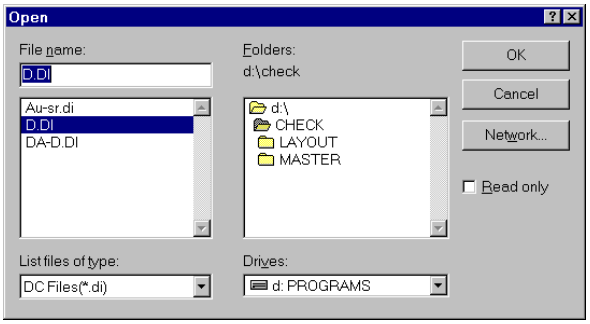

Figure 9.8. Open dialog box for opening a file *filename.DI*.

9.2.5 Output files of *DC*

DC always creates two output files: the archive file, *filename.DO*, and the graphic file, *filename.DG*. The file *filename.DO* is a text file and can be examined using any text editor. This file has three main functions, to record the input data, to record the whole computational process and results, and to record error messages when run-time errors occur. The archive file also includes the graphic data of 2D or 3D contours to be used by the visualization program *DP*. A text file for creating the electron density images, *filename.DG*, is always created after running the *DC* program. It contains electron densities calculated for every mesh-point in the real space. The Cartesian coordinates of the atoms of a unit cell are also stored in the file *filename.DG*, which is the only input file needed for running the *DP* program.

9.2.6 Limitations of *DC*

The dynamic memory management is employed in *DC*. There are a few limitations of *DC* to note. The number of nearest neighbor unit cells to include for lattice sums should be less than 11. The largest mesh grid is 30x30. The maximum number of atoms allowed for a unit cell is 500. The maximum numbers of atomic orbitals for a unit cell are 1,500. Since the contribution to the electron density due to the atoms, which locate beyond the FPZ, must be considered in order to get correct and

smooth boundaries of the density plot, the maximum orbital number should be somewhat less than 1500.

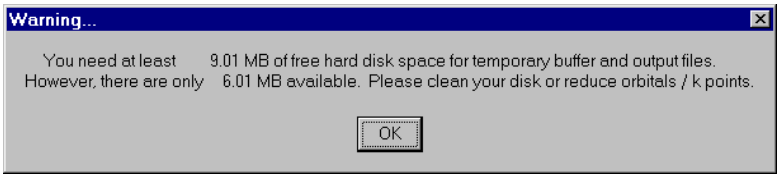

Figure 9.9. Warning message calling for the cancellation of a huge computational job.

During the execution of *DC*, a number of temporary files named *DC.n* are generated, where n is an integer between 1 and 99. The sizes of these files dramatically increase with increasing the number of atoms in a unit cell and the number of k points to be calculated. *CAESAR* provides a utility program to compare the size requirements for the requested computation with the available memory and space. All the information will be automatically detected from the input file and the computer system. If the requirements are not met, a warning message is displayed on the screen (*Figure 9.9*), which allows one to cancel the job before starting it.

9.3 Electron density display program *DP*

When the *DP* program is loaded with a proper *filename.DG* file, the *DP* window appears (*Figure 9.10*). The menus of this window include *File*, *2D*, *3D*, *Extend*, *Export*, *Zoom*, *Preference*, and *Save*. The functions of these menus are described below.

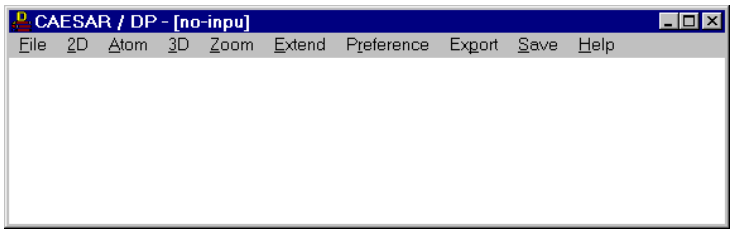

Figure 9.10. Window of *DP*.

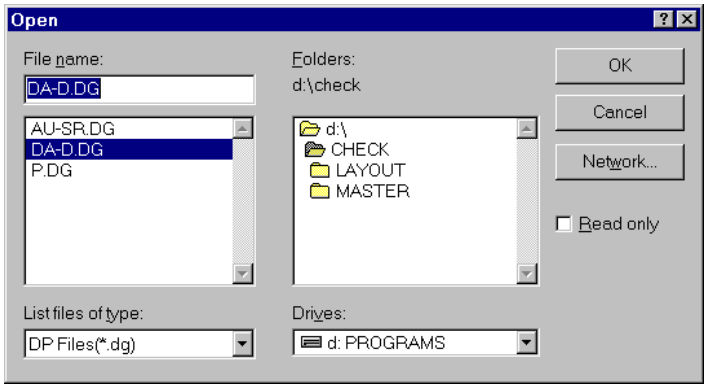

Figure 9.11. *Open* dialog box for opening a graphic file *filename.DG*.

•***File***

When the *DP* program is launched, the *Open* dialog box appears to allow the user to select a *filename.DG* file (*Figure 9.11*). The user can open a new input file by using the *Open* command of the *File* menu. When a new input file is selected, the previously selected one is closed, and the screen display is updated with the new data. The user may exit *DP* by using the *Exit* command.

•***2D***

This menu provides two options of presenting an electron density plot, *Contour-line* and *Gray-scale*.

Contour-line:

This command displays a 2D contour plot on screen. The default setting shows 7 contour lines projected on the cross-section plane, with the highest-lying atoms displayed as circles. The contour values are shown at the top right corner of the screen (*Figure 9.12*).

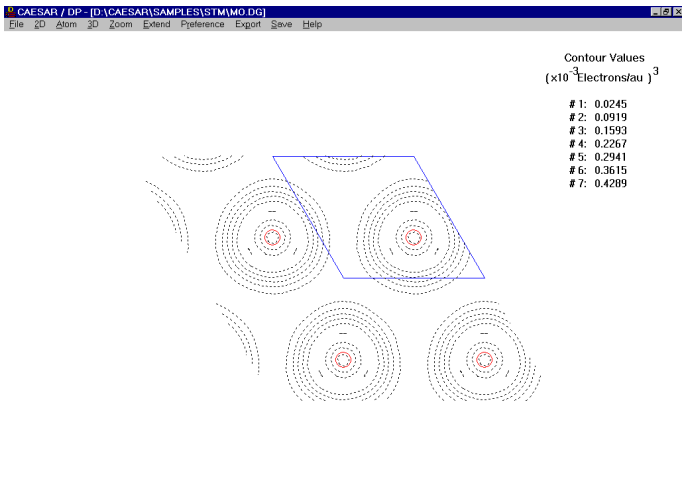

Figure 9.12. Contour representation of a 2D $\rho\,(r_0, e_f)$ plot.

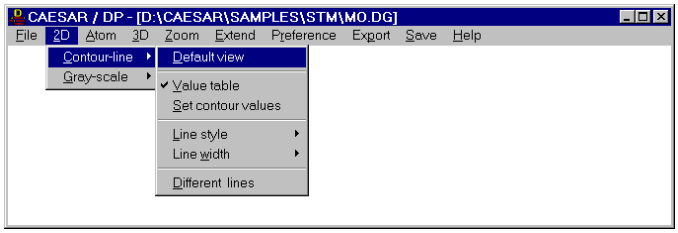

Figure 9.13. Items of the *Contour-line* menu.

The *Contour-line* command has four groups of options by which to modify the 2D contour plot displayed on the screen (*Figure 9.13*). When checked, the item *Value table* show the contour values at the top-right corner of the screen. The item *Set contour values* allows the user to change the contour pattern by opening the *Set Contour Values* dialog box (*Figure 9.14*). The *Default* button in the box provides seven contour lines whose values are evenly spaced between the maximum and the

minimum densities. The *Customize* button activates the parameter field lying below, which shows the seven contour values used for the default setting. The user can include up to 16 contours with values lying between the minimum and the maximum values.

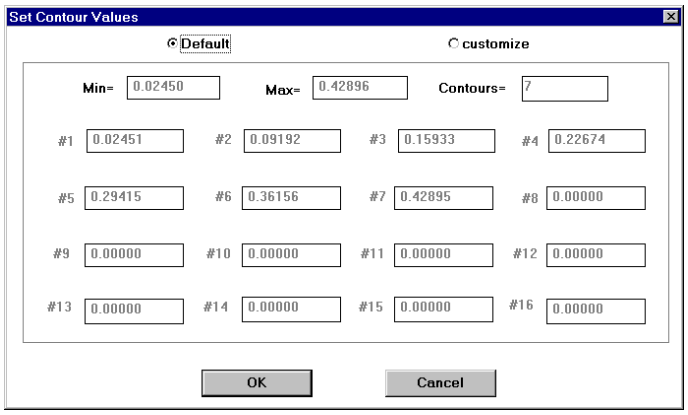

Figure 9.14. Set Contour Values dialog box.

The item *Line style* gives two choices, *Dotted* and *Solid*, for drawing contour curves. The item *Line width* provide three pen widths, *1x*, *2x* and *3x*, for drawing contour lines.

The program *DP* displays contour lines with uniform width and same color. If the user wants to emphasize the difference between different contour lines, the item *Different lines* creates contours with different color intensities.

Gray-scale:

This command displays an electron density plot in gray scale. It has three groups of options by which to modify the plot displayed on the screen (*Figure 9.15*).

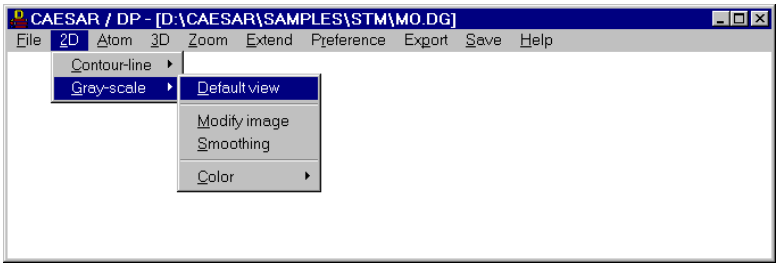

Figure 9.15. Items of the *Gray-scale* menu.

The item *Default view* shows a gray-scale image in red, in which the density differences are represented in terms of different intensities of red (*Figure 9.16*) with the color intensity scaling bar at the upper right corner.

The item *Modify image* provides a way of editing images. It opens the *Modify Density* dialog box (*Figure 9.17*), which allows the user to change the color intensity scaling. To non-linearly increase the color intensity of the darker region of a gray-scale image, it is necessary to use a number larger than 1 in the *Raising Density* field. This is useful in examining the atoms which do not contribute strongly to the electron density on the surface (*Figure 9.18*). The item *Smoothing* instructs the *DP* program to employ a better fitting algorithm for removing unrealistic density spots that result from fitting procedures. This function takes a longer fitting time than the default fitting procedure.

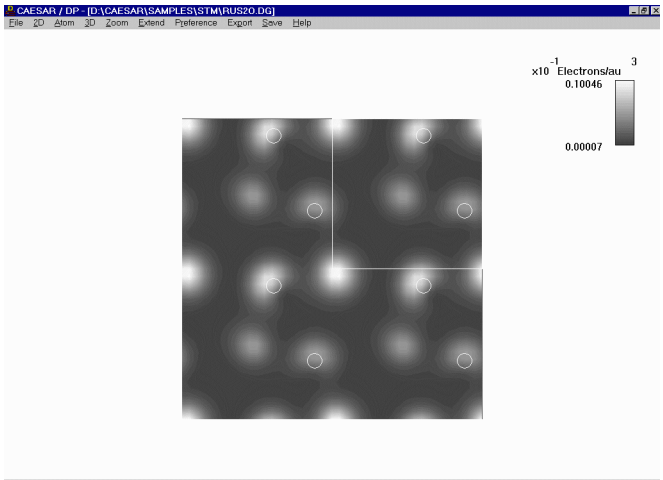

Figure 9.16. Gray-scale representation of a 2D $\rho\,(r_0, e_f)$ plot.

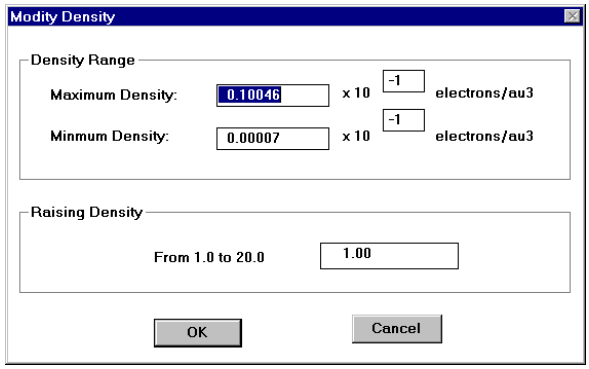

Figure 9.17. *Modify Density* dialog box.

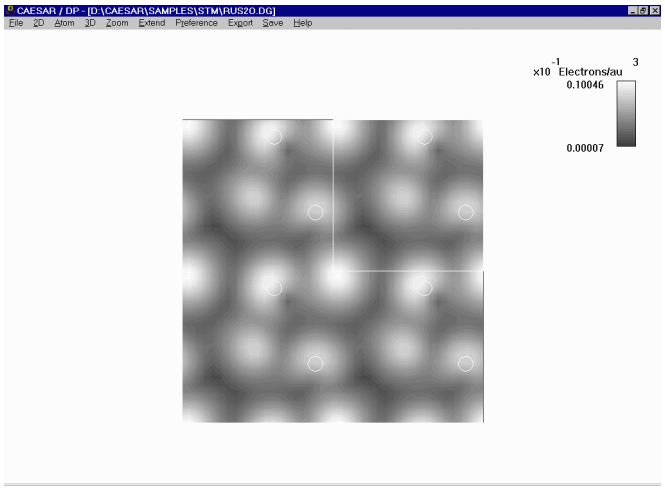

Figure 9.18. Gray-scale representation of a 2D $\rho\,(r_0, e_f)$ plot with enhanced densities.

The item *Surface color* provides 5 color options, i.e., *Red*, *Green* *Blue*, *Gray* and *Customize* (*Figure 9.19*). The *Customize* option opens the *Define Surface Color* dialog box (not shown), which allows the user to assign two colors for the lowest and the highest densities. Each color is defined in terms of three numbers for *Red*, *Green* and *Blue*.

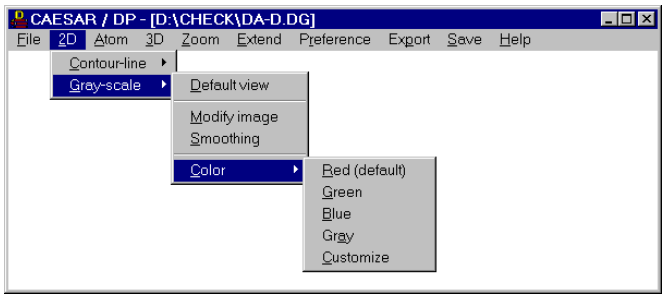

Figure 9.19. Items of the *Color* menu.

•*Atom*

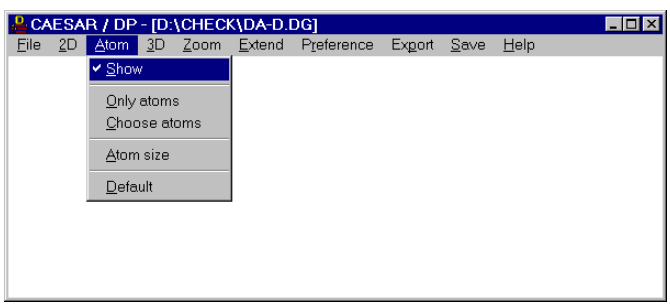

Figure 9.20. Items of the *Atom* menu.

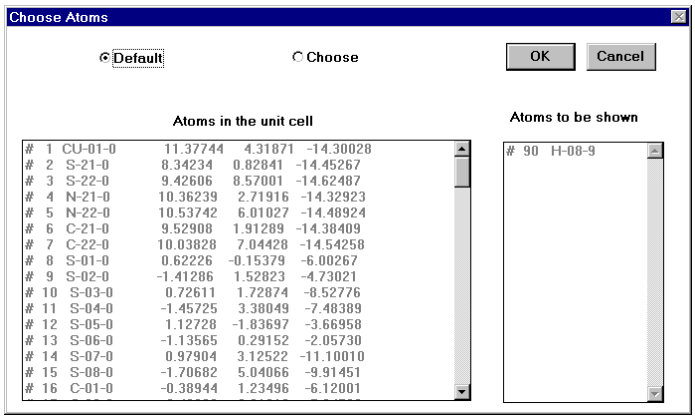

Figure 9.21. *Choose Atoms* dialog box.

This menu provides several modes of showing the atoms (*Figure 9.20*). When the item *Show* is checked, the atoms selected either by *Default* (i.e., the highest-lying atoms) or by the user employing

the *Choose atoms* command are displayed on the screen as circles. The *Choose atoms* command opens the *Choose Atoms* dialog box (*Figure 9.21*), where the names of all unit cell atoms and their coordinates are listed in the *Atoms in the unit cell* field, while the atoms to be shown on the screen are listed in the *Atoms to be shown* field. To change the default, click the *Choose* button to activate the two fields. Then click the selected atoms in the *Atoms in the unit cell* field to remove them, and select the needed atoms from the *Atoms in the unit cell* field by clicking. After completing the selection, click the *OK* button to save this setting and display the selected atoms.

The command *Only atoms* remove all contour lines from a contour-line plot, but it does not affect a gray-scale plot nor a 3D representation of an electron density plot (see below) and the gray-scale plots.

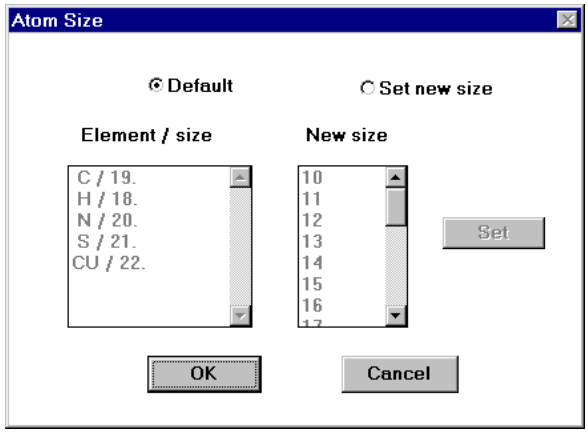

Figure 9.22. Atom Size dialog box.

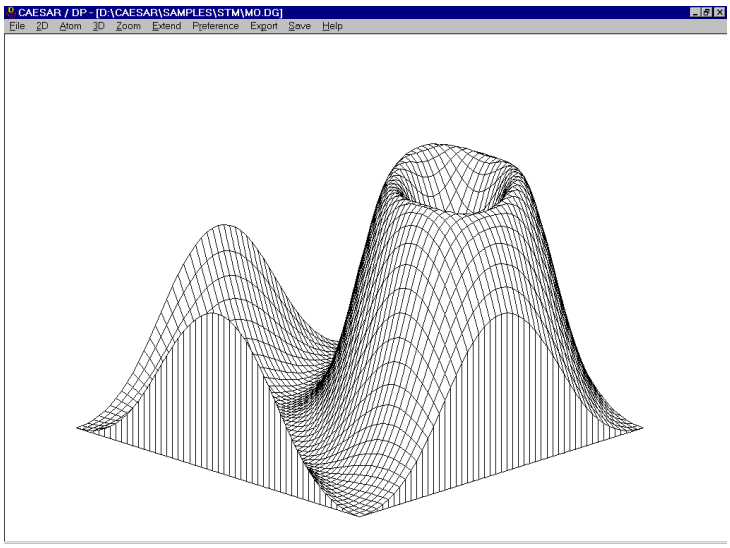

Figure 9.23. 3D $\rho\,(r_0, e_f)$ plot.

The *Atom size* command opens the *Atom Size* dialog box (*Figure 9.22*), which allows the user to assign arbitrary sizes to different atoms. The *Element/size* field lists all the elements of a unit cell and their default sizes. The *New size* field lists all available sizes that can be assigned to different elements. The two fields are activated by clicking the *Set new size* button. To change the size of one specified

element, the user should select the element from the *Element/size* field and the desired size from the *New size* field, and then click the *Set* button to save the setting.

•*3D*

This menu converts a 2D representation of an electron density plot into a 3D representation (*Figure 9.23*), in which the third dimension represents the electron density. The *Default* view uses the top-view angle of 25 degrees and the height scaling factor of 1.0. This setting can be reset by using the *Height scale* and *Rotation angle* commands.

•*Zoom*

This menu provides scaling factors for enlarging or reducing the size of an electron density plot (*Figure 9.24*). The available zoom-out factors are 25%, 50% and 75%, while the available zoom-in factors are 125%, 150 and 175%. The default scaling factor is 100%.

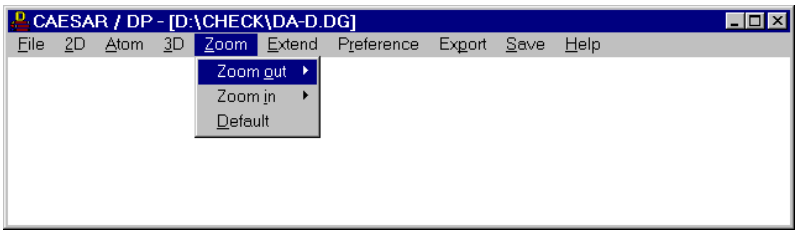

Figure 9.24. Items of the *Zoom* menu.

•*Extend*

To examine the topological features of an electron density plot, it is convenient to repeat a satisfactory view of the plot that the user obtains after zooming and other refining operations.

The extending occurs only along the 2D vectors (i.e., **a** and **b**, **a** and **c**, or **b** and **c**) used to obtain a 2D contour-line or a 2D gray-scale plot. There are three options of extension , i.e., 6x6, 10x10 and 14x14. The *Default* option will show a 2x2 plot (*Figure 9.25*). The 3D representation of an electron density plot cannot be extended.

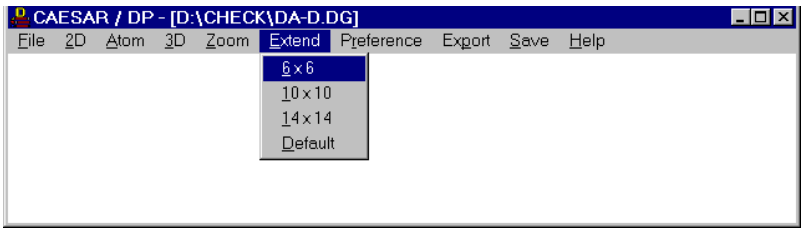

Figure 9.25. Items of the *Extend* menu.

•*Preference*

Some features of graphics can be reset by selecting the commands of the *Preference* menu (*Figure 9.26*).

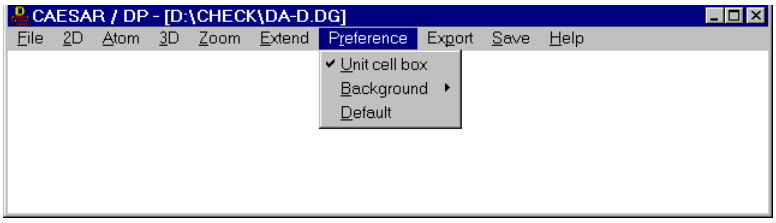

Figure 9.26. Items of the *Preference* menu.

When checked, the command *Unit cell box* shows the unit cell boundary (*Figure 9.27*). The *Background* command provides five different colors, *White*, *Black*, *Red*, *Green* and *Blue*, for the screen background (*Figure 9.28*).

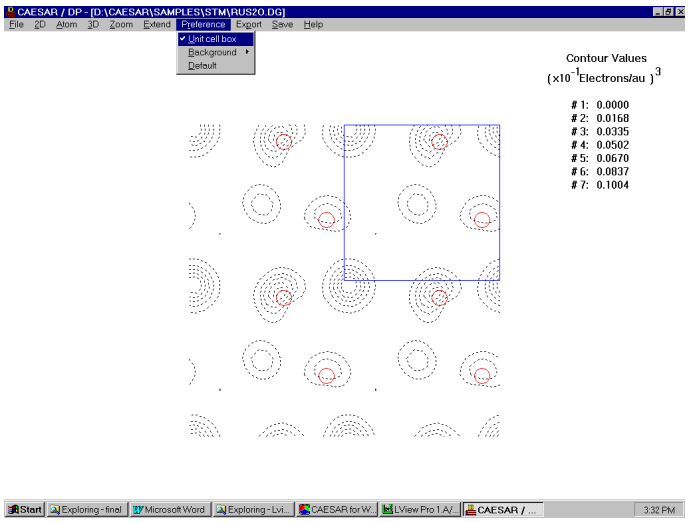

Figure 9.27. *Unit cell box* command.

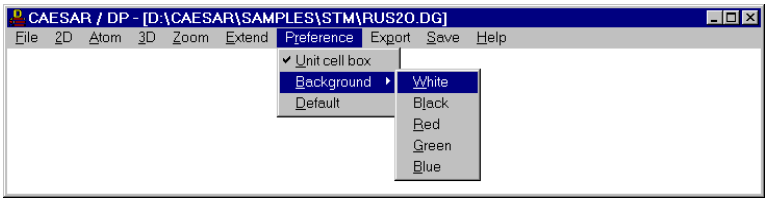

Figure 9.28. Items of the *Background* menu.

The *Default* command restores the default choice for an electron density plot, i.e., a 2D contour-line plot with 2x2 unit cells, 100% zooming rate, and the highest-lying atoms.

•*Export*

This menu provides two ways of saving the images on the screen as permanent files. A contour-line or 3D representation plot can be saved in the *PostScript* format (see below). However, a gray-scale image should be saved as a *Bitmap* or *TIFF* file *(Figure 9.29)* by using the command *Bitmap* or *TIFF*. It takes a while to write an output file *filename.BMP* or *filename.TIF*. A 2D contour-line plot

can be saved with the bitmap or tiff format, but it is better to save it with the PostScript format because the latter provides a much higher resolution.

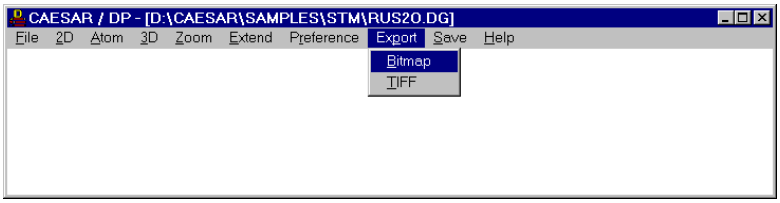

Figure 9.29. Items of the *Export* menu.

•*Save*

The user can employ this menu to save an electron density plot on the screen in a PostScript file *filename.DP*. The program will confirm the drive, path and file name by displaying a dialog box (*Figure 9.30*). If the file name already exists, another dialog box will appear to ask the user to confirm the overwriting action.

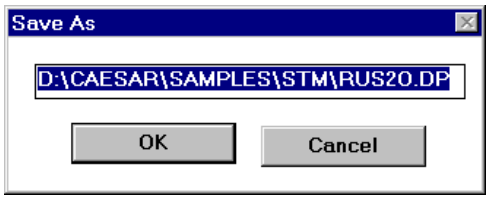

Figure 9.30. Save As dialog box for saving a file *filename.DP*.

The user can save several different pictures in one *filename.DP*. Each picture is saved as one full page. Once a *filename.DP* has been created, many pages can be appended to it. Before appending a new picture, the program will ask the user to confirm appending action or to open a new *filename.DP*.

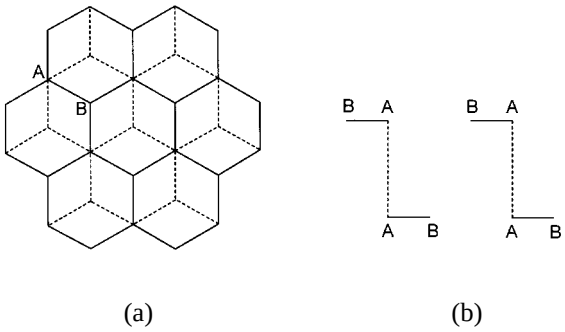

Figure 9.31. Schematic representation of the arrangement between two adjacent graphite sheets in HOPG: (a) top projection view, where the C-C bonds of the upper and lower sheets are indicated by solid and broken lines, respectively; (b) side projection view, where the interlayer C···C contact are shown by dotted lines.

9.4 Examples

9.4.1 Graphite [1]

Adjacent layers of highly ordered pyrolytic graphite (HOPG) are arranged in such a way that there occur two types of carbon atoms (A and B) on the surface layer (*Figure 9.31*). The A-site carbon atoms lie directly above the carbon atoms of the underlying layer, and the B-site carbon atoms are located above the centers of the carbon hexagons of the underlying layer.

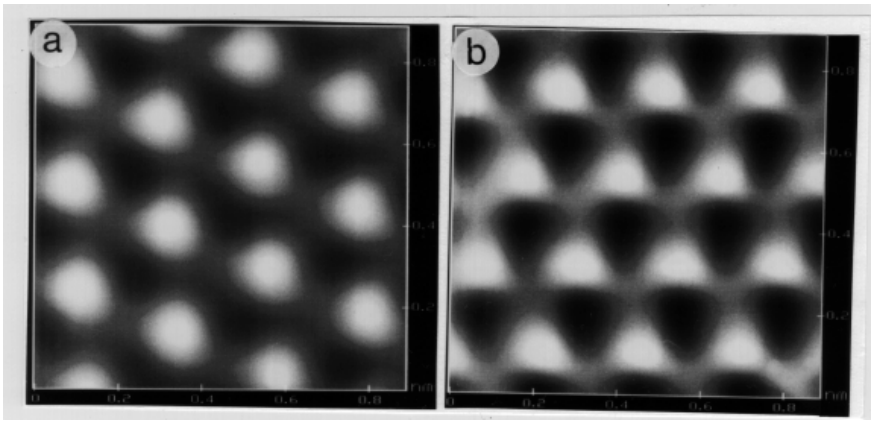

Figure 9.32. (a) STM current image of HOPG (I_{set} = 2 nA, V_{bias} = 28 mV). (b) AFM height image of HOPG.

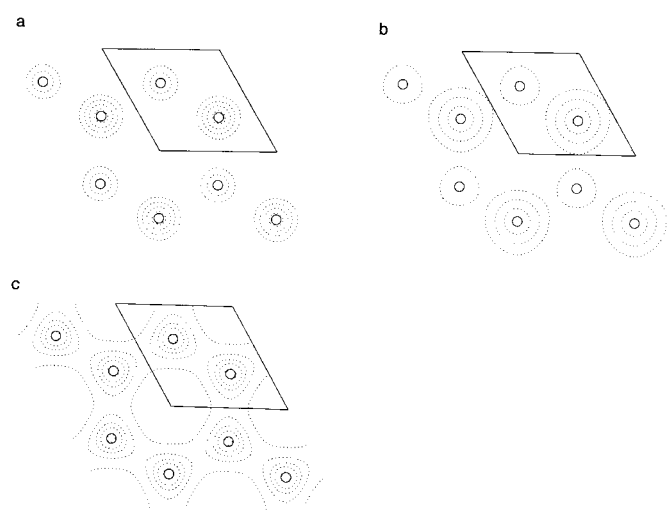

Figure 9.33. Partial and total density plots calculated for the graphite bilayer (a) $\rho(r_0, e_f)$ plot for $V_{bias} > 0$. The contour values used are 1.0 x 10^{-2}, 1.5 x 10^{-2}, 2.0 x 10^{-2} and 2.5 x 10^{-2} electron/au^3. (b) $\rho(r_0, e_f)$ plot for $V_{bias} < 0$. The contour values used are 1.0 x 10^{-3}, 2.5 x 10^{-3}, 5.0 x 10^{-3} and 7.5 x 10^{-3} electron/au^3. (C) $\rho(r_0)$ plot. The contour values used are 1.0 x 10^{-1}, 1.5 x 10^{-1}, 1.8 x 10^{-1}, 2.0 x 10^{-1} and 2.2 x 10^{-1} electron/au^3.

Most STM images of HOPG show a hexagonal pattern of bright spots, which are assigned to three nonadjacent carbon atoms for each carbon hexagon forming the surface graphite layer (*Figure 9.32a*). The "three-for-hexagon" patterns that are obtained for positive and negative bias voltages have an identical peak registry, i.e., the bright spots of a positive bias image are the same as those of a negative bias image.[5]..The STM and AFM images of HOPG are simulated by calculating the partial and total density plots, $\rho(r_0, e_f)$ and $\rho(r_0)$, for a graphite bilayer (*Figure 9.33*), respectively.

In the CAESAR\Examples\Chapter9\Graphite directory, the *BC*, *PC*, *DC* input files for STM image simulation are *Gr-STM.BI*, *Gr-STM.PI* and *Gr-STM.DI*, respectively, while those for AFM image simulation are *Gr-AFM.BI*, *Gr-AFM.PI* and *Gr-AFM.DI*, respectively.

The high electron density spots of the $\rho(r_0, e_f)$ plot are located at the B-site carbons for the sample-to-tip and tip-to-sample tunneling (*Figure 9.33*). As depicted in *Figure 9.34* for a graphite bilayer, this comes about because the π-band levels of HOPG around the Fermi level have more contributions from the B-site carbons than from the A-site carbons (see also *Section 7.5.2*). Another factor contributing the three-for-hexagon pattern is the tip-force induced surface corrugation.[6]

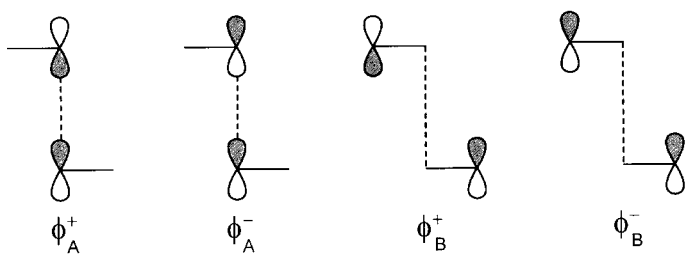

(a)

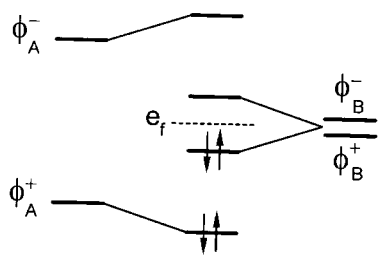

(b)

Figure 9.34. (a) Four group orbitals resulting from each unit cell of the graphite bilayer. (b) Orbital interactions between the Bloch orbitals derived from ϕ_A^+ and ϕ_A^- with those derived from ϕ_B^+ and ϕ_B^-, respectively, leading to the band orbitals of the graphite bilayer. The Fermi level reflects that there are four π-electrons per unit cell.

The total electron density plot $\rho(r_0)$ calculated for HOPG shows no difference in the electronic density at the A- and B-sites, because the total electron density plot is based on all the occupied band levels (*Figure 9.33c*). However, this pattern is not in agreement with observed AFM images, which show a three-for-hexagon pattern as do observed STM images. The bright spots of AFM images are

also represented by the B-site carbons. This discrepancy arises because the tip force induces a surface corrugation in which the z-heights of the A-site carbons are depressed more than are the B-site carbon atoms during the scanning.[6]

9.4.2 β-Nb_3X_8 (X = Cl, Br, I) [1,7]

β- Nb_3X_8 (X = Cl, Br, I) is a layered compound. In the Nb-atom sheet of each Nb_3X_8 layer, the Nb atoms form triangle Nb_3 cluster, so that each Nb atom is in a distorted octahedral environment. In each Nb_3X_8 layer, the top and bottom sheets of X atoms are not equivalent. On the bottom halogen sheet containing that X(2) and X(4) atoms in *Figure 9.35* (surface A), the X(4) atoms lie farther away from the Nb-atom sheet than the X(2) atoms (by 0.60, 0.55, and 0.50 Å for X = I, Br and Cl, respectively). On the top halogen sheet containing the X(1) and X(3) atoms in *Figure 9.35* (surface B), the X(1) atoms lie farther away from the Nb-atom sheet than the X(3) atoms (by 0.44, 0.33, and 0.35 Å for X = I, Br and Cl, respectively). In principle, the surface of Nb_3X_8 observed by STM and AFM can be either surface A or surface B.

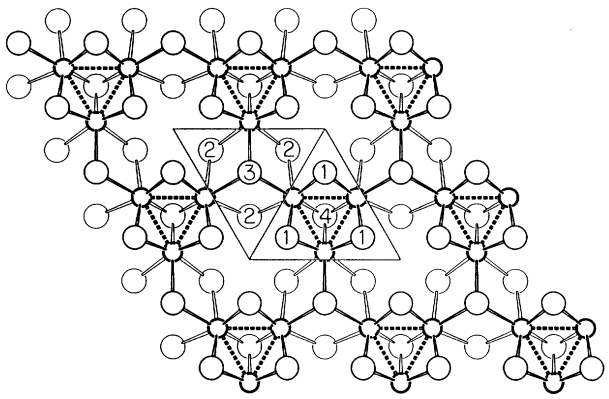

Figure 9.35. Schematic projection view, along the crystallographic c-axis direction, of a single Nb_3X_8 layer. The Nb and X atoms are represented by small and large circles, respectively. The Nb_3 clusters in the Nb-atom sheet are shown by connecting the Nb atoms with broken lines.

Figure 9.36a shows an atomic-resolution AFM image obtained for β-Nb_3I_8. This image exhibits the unit cell pattern consisting of one bright spot and three less bright ones, and this pattern resembles the atomic arrangement of surface A. The STM images, recorded on the same crystal surface of β-Nb_3I_8, are shown in *Figure 9.36b*. A zoomed and filtered part of this STM image reveals three brighter triangular spots and a less pronounced one per unit cell (*Figure 9.36c*).[7]

In the CAESAR\Examples\Chapter9\Nb3I8 directory, the *BC*, *PC* and *DC* input files for the simulation of STM images are *STM.BI*, *STM.PI* and *STM.DI*, respectively. The corresponding files for the AFM image simulation are *AFM.BI*, *AFM.PI* and *AFM.DI*.

Figure 9.37a shows the dispersion relations of the d-block energy bands calculated for a single Nb_3X_8 layer (nine t_{2g} block bands lying in the vicinity of the Fermi level). With the oxidation state I^-, there are seven electrons to fill the bottom four bands of *Figure 9.37a*. The highest occupied band, which is somewhat narrow, is half-filled. The $\rho(r_0)$ and $\rho(r_0, e_f)$ plots of a single Nb_3I_8 layer calculated for surface A are shown in *Figures 9.38a* and *9.38b*, respectively. Within the unit cell of the

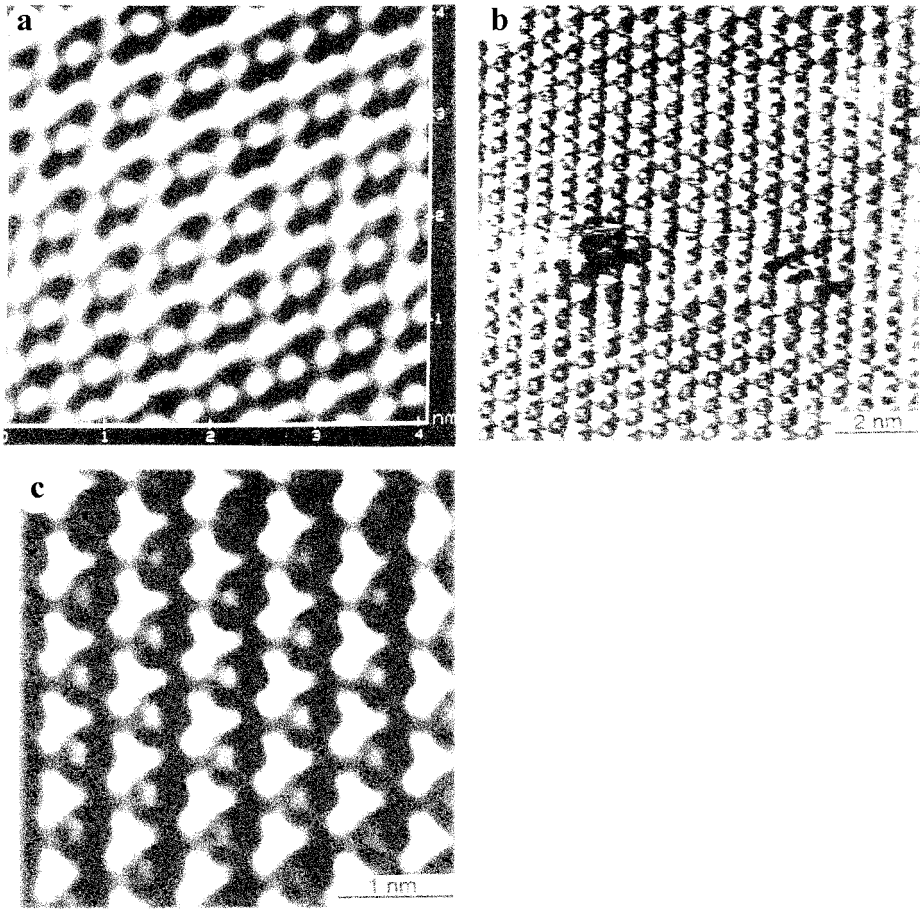

Figure 9.36. (a) AFM height image of β-Nb_3I_8; (b) STM current images of β-Nb_3I_8, (I_{set} = 0.75 nA, V_{bias} = 180 mV); (c) after FFT filtering.

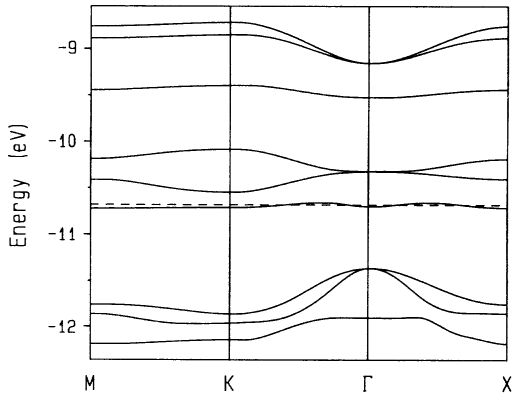

Figure 9.37. (a) Dispersion relations of the nine bands, in the vicinity of the Fermi Level (shown by the broken line), calculated for a single Nb_3I_8 layer of β-Nb_3I_8.

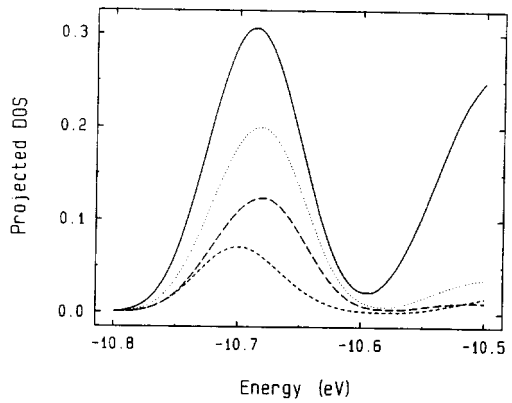

(b)

Figure 9.37. (b) PDOS values of the iodine atoms of surface A, in the energy region of the half-filled band, calculated for a single Nb_3I_8 layer of β-Nb_3I_8. The curves represent the p_z orbital of I(2) by the dotted line, the p_x and p_y orbitals of I(2) by the solid line, the p_z orbital of I(4) by the dashed line, and the p_x and p_y orbitals of I(4) by the long dashed line.

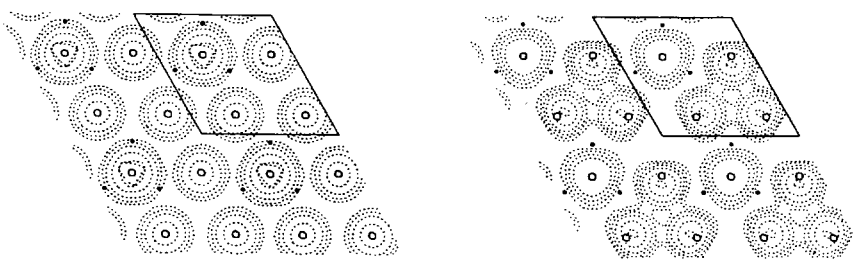

(a) (b)

Figure 9.38. (a) $\rho\ (r_0)$ and (b) $\rho\ (r_0, e_f)$ plots calculated for surface A of a single Nb_3I_8 layer of β-Nb_3I_8. The plot area consists of four unit cells, and a unit cell is indicated by the rhombus. For clarity, the I atoms on the opposite surface are not shown. The Nb atom and I atoms are shown by small and large circles, respectively. The contour values used are 85 x 10^{-3}, 50 x 10^{-3}, 20 x 10^{-3}, 10 x 10^{-3} and 5 x 10^{-3} electron/au^3 in (a) and 100 x 10^{-5}, 50 x 10^{-5}, 20 x 10^{-5}, 10 x 10^{-5}, 5 x 10^{-5} and 2.5 x 10^{-5} electron/au^3 in (b).

$\rho(r_0)$ plot, one atom has a higher density than the other three atoms, in agreement with AFM image of *Figure 9.36a*. The $\rho(r_0, e_f)$ plot, obtained by sampling all levels of the half-filled band of *Figure 9.37a*, is consistent with the STM pattern of *Figure 9.36c*. In each unit cell of this plot, the three I(2) atoms have a greater density than do the I(4) atom, although the I(2) atoms lie farther away from the tip by 0.60 Å. As shown by the DOS analysis of *Figure 9.37b*, this reflects the fact that the highest occupied band has a stronger contribution from the I(2) atoms than from the I(4) atoms. In addition, in

the $\rho(r_0, e_f)$ plot, the density peaks of the three I(2) atoms within a unit cell are closer to one another than expected on the basis of the crystal structure. This effect is caused by the hybridization of the I(2) atom p-orbitals in the half-filled band, and it explains the observation of triangular bright spots in the STM image in *Figure 9.36c*.

9.4.3 (100) Surface of $SrTiO_3$ [8]

The structure of $SrTiO_3$ has alternating layer of TiO_2 and SrO. Auger electron spectroscopy analyses [9] indicate that the TiO_2 plane constitutes most of the top layer of vacuum fractured $SrTiO_3$ sample. Ultraviolet photoemission spectroscopy studies show that the electronic properties of $SrTiO_3$ (100) are strongly influenced by oxygen vacancies on the surface TiO_2 plane.[10] STM studies of $SrTiO_3$ (100) (annealed at high temperatures) in ultrahigh vacuum (UHV) led to atomic scale resolution images with $\sqrt{5}x\sqrt{5}$ superstructures.[10b] The bright spots of these images were suggested to correspond to the oxygen vacancies.[10]

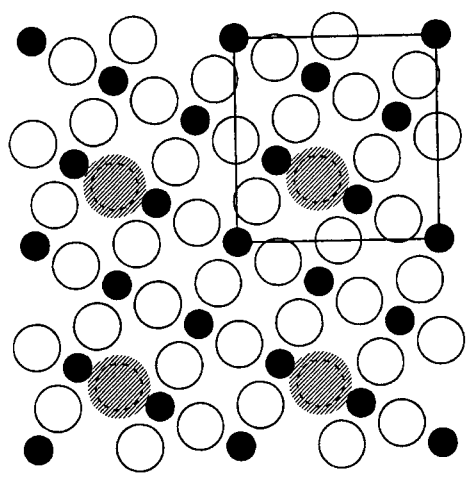

Figure 9.39. Model of a $SrTiO_3$ (100) surface with ordered $\sqrt{5}x\sqrt{5}$ oxygen vacancy. The Ti atoms are represented by small filled circles, the oxygen atoms by large empty circles, and the oxygen vacancies by shaded broken circles. The square box represent a unit cell.

The model of a $SrTiO_3$ (100) surface with ordered $\sqrt{5}x\sqrt{5}$ oxygen vacancy is shown in *Figure 9.39*. The top Ti-O layer of this surface has a unit cell, Ti_5O_9, which contains one oxygen vacancy. By capping the Ti atoms of this "Ti_5O_9" layer with axial oxygen atoms from underneath, one obtains the layer with unit cell formula Ti_5O_{14}. There are two kinds of Ti atoms in this "Ti_5O_{14}" layer. The Ti atoms nonadjacent to the oxygen vacancies have a C_{4v} site symmetry (see the TiO_5 fragment in *Figure 9.40a*) and are in the oxidation state Ti^{4+}. The Ti atoms adjacent to the surface oxygen vacancies have a C_{2v} site symmetry (see the TiO_5 fragment in *Figure 9.40b*) and are in the oxidation state Ti^{3+}. One oxygen atom vacancy creates two Ti^{3+} sites, as depicted by the fragment in *Figure 9.40c*. Given the oxidation state O^{2-} for all oxygen atoms, the charge appropriate for the Ti_5O_{14} layer is -10 to have three Ti^{4+} and two Ti^{3+} ions per unit cell. Likewise, the charges for the TiO_5, TiO_4 and

Ti_2O_8 fragments are TiO_4^{5-}, TiO_4^{5-} and $Ti_2O_8^{10-}$, respectively. One may construct the structures of the $Ti_5O_{14}^{10-}$ layer and the TiO_5^{6-}, TiO_4^{5-} and $Ti_2O_8^{10-}$ fragments as found in the bulk crystal structure of $SrTiO_3$. Such structures will be referred to as unrelaxed structures. In the CSASAR\Examples\Chapter9\SrTiO3 directory, the *BC*, *PC* and *DC* input files for the unrelaxed $Ti_5O_{14}^{10-}$ layer are *U.BI*, *U.PI* and *U.DI*, respectively.

In the UHV STM experiments, the images were recorded with positive bias voltage so that the energy region of interest for $\rho(r_0, e_f)$ plot calculations of the $Ti_5O_{14}^{10-}$ layer is the unoccupied energy levels lying in the vicinity of the Fermi level. In general, a large tip-sample distance is involved in UHV than in ambient-condition STM imaging.

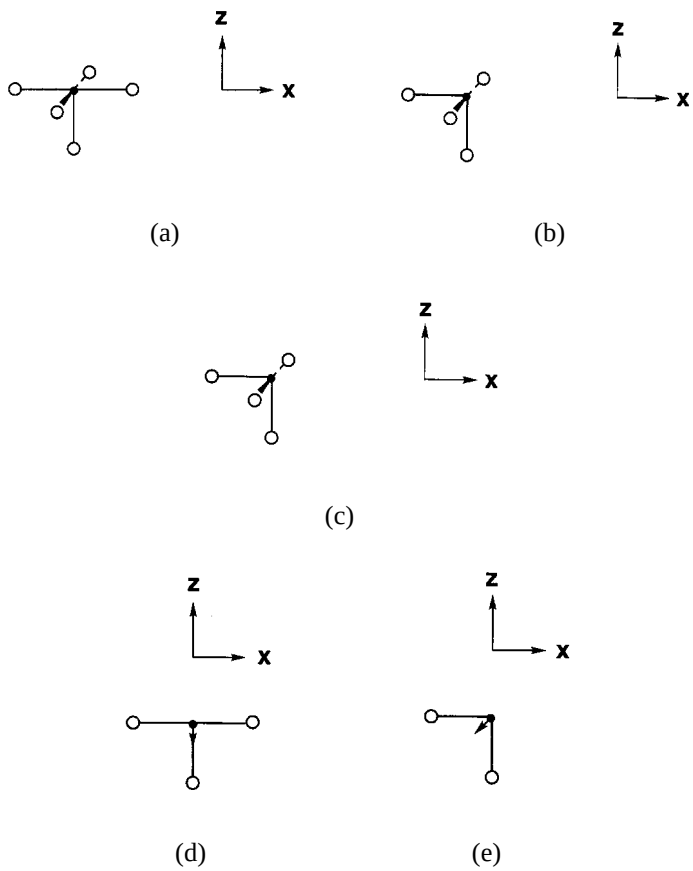

Figure 9.40. (a) Structure of a TiO_5^{6-} fragment representing a Ti^{4+} site of the $SrTiO_3$ (100) surface. (b) Structure of a TiO_4^{5-} fragment representing a Ti^{3+} site of the $SrTiO_3$ (100) surface. (c) Structure of a $Ti_2O_8^{10-}$ fragment representing two Ti^{3+} sites of the $SrTiO_3$ (100) surface. (d) Displacement of Ti atoms expected at Ti^{4+} site of the $SrTiO_3$ (100) surface. (e) Displacement of Ti atoms expected at Ti^{3+} site of the $SrTiO_3$ (100) surface. For simplicity, only the atoms lying on the xz-plane are shown in (d) and (e).

For calculations, all the unoccupied band levels lying within 0.25 eV from the Fermi level (i.e., the energy window $\Delta = 0.25$ eV) were employed. The $\rho(r_0, e_f)$ plot calculated for $r_0 = 3.0$ Å shows a four-spot density pattern around each Ti site (*Figure 9.41a*). The four spots around each Ti atom are merged into a doughnut shape for smaller values of r_0 such as 1 and 2 Å. This patterns arises because

in this energy region the band levels have “xz” and “yz” orbital contributions from each Ti center. However, this $\rho(r_0, e_f)$ plot is not consistent with the observed STM image.

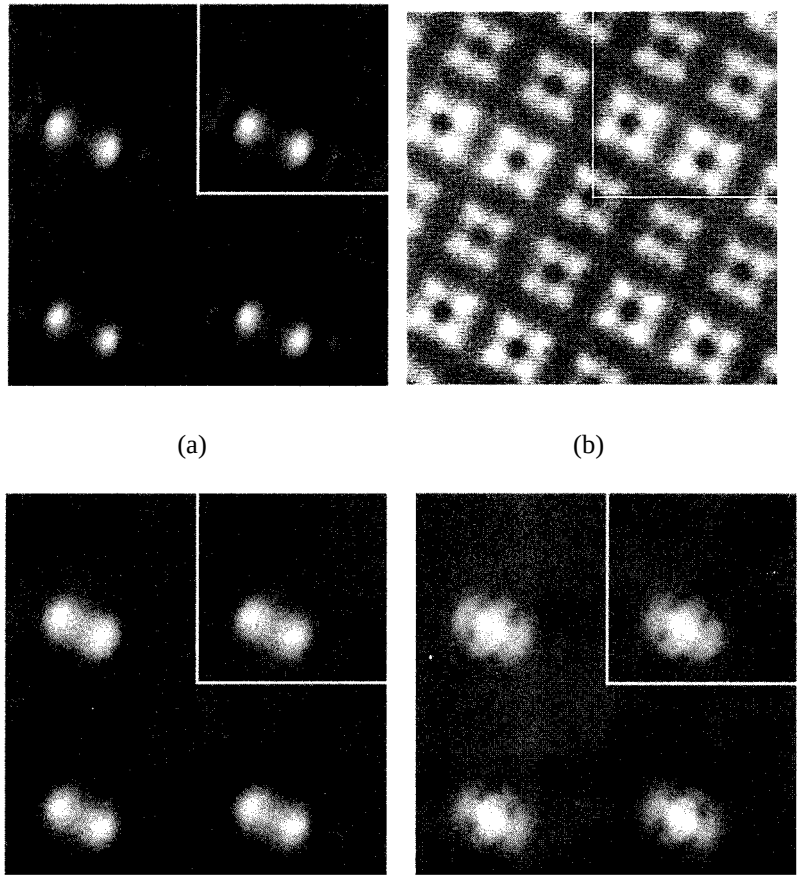

(a) (b)

(c) (d)

Figure 9.41. $\rho(r_0, e_f)$ plot calculated for (a) the unrelaxed $Ti_5O_{10}^{14-}$ at $r_0 = 3.0$ Å and (b) for the relaxed $Ti_5O_{10}^{14-}$ at $r_0 = 1.0$ Å, (c) $r_0 = 2.0$ Å and (d) $r_0 = 3.0$ Å. The contrast covers electron density variations in the 1.3 - 6.1x10^{-5} electrons au^{-3} range in (a), 0.0 - 2.3x10^{-3} electrons/au^3 range in (b), 0.0 - 1.4x10^{-4} electrons/au^3 range in (c), and 0.0 - 5.4x10^{-5} electrons/au^3 range in (d).

A probable geometry relaxation around the Ti^{3+} and Ti^{4+} sites might affect the bottom portion of the d-block bands of the $Ti_5O_{14}^{10-}$ layer. In transition metal compounds of ML_5 square pyramids with d^0 or d^1 ions, the empty d orbitals of the metal ions are used to stabilize the filled p orbitals of the surrounding ligands.[11] This interaction is enhanced when the metal ion moved away from the L_4 basal plane toward the axial ligand. Thus it is expected that the Ti^{4+} (d^0) ion in a C_{4v} TiO_5^{6-} unit moves out of the O_4 basal plane toward the axial oxygen atom (*Figure 9.40d*). Similarly, the Ti^{3+} (d^1) ion of a C_{4v} TiO_4^{5-} unit is expected to move in the xz-plane to decrease both Ti-O bonds of the plane (*Figure 9.40e*) equally. For our qualitative discussion, we introduce a Ti atom displacement of 0.2 Å at the Ti^{4+} and

Ti^{3+} sites of the unrelaxed $Ti_5O_{14}^{10-}$ layer, as defined in *Figures 9.40d* and *9.40e*. The resulting layer will be referred to as the relaxed $Ti_5O_{14}^{10-}$ layer. In the CARSAR\Examples\TiO directory, the *BC*, *PC* and *DC* input files for the relaxed $Ti_5O_{14}^{10-}$ layer are *R.BI, R.PI* and *R.DI*, respectively.

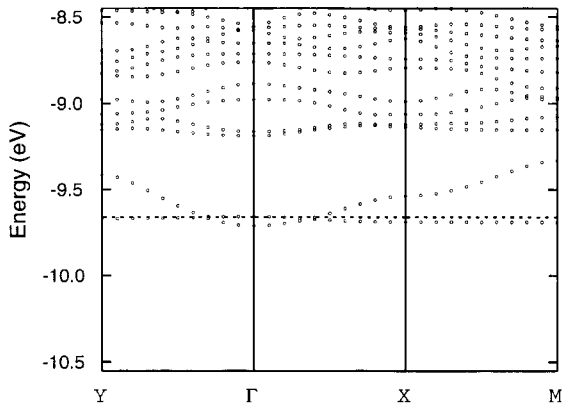

(a)

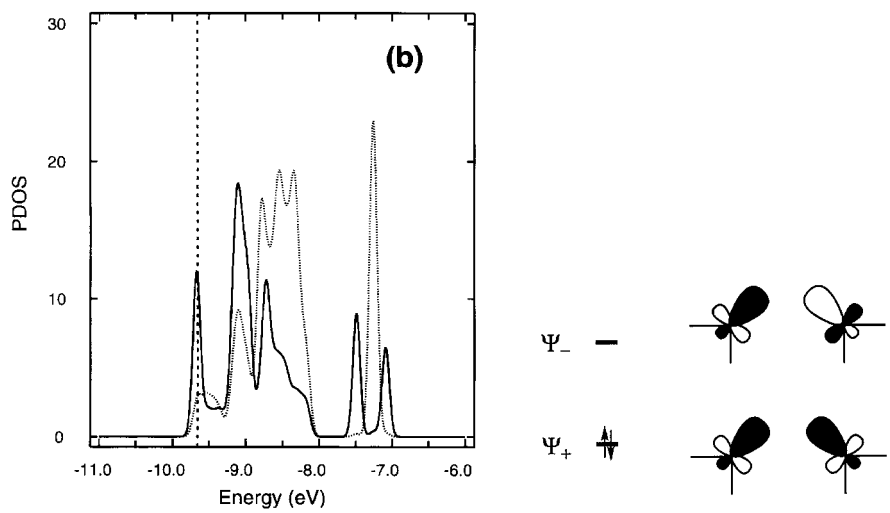

(b) (c)

Figure 9.42. Electronic structure of the relaxed $Ti_5O_{10}^{14-}$ layer. (a) Dispersion relations of the bottom portion of the d-block bands, where the dashed line represnets the Fermi levels. (b) PDOS plots calculated for the Ti^{3+} and Ti^{4+} sites. The solid and dotted lines represent the Ti^{3+} and Ti^{4+} contributions, respectively. (c) Bonding and antibonding orbitals ψ_+ and ψ_- of a $Ti_2O_8^{10-}$ fragment resulting from the lowest lying hybridized d orbital of Ti^{3+} site.

Figure 9.42a shows the dispersion relations of the bottom portion of the d-block bands calculated for the relaxed $Ti_5O_{14}^{10-}$ layer. Unlike the case of an unrelaxed $Ti_5O_{14}^{10-}$ layer, the

bottom flat band of *Figure 9.42a* overlaps with one dispersive band. The major component of this bottom dispersive band is the "xy" orbital of each metal atom. The PDOS plots calculated for the Ti^{3+} and Ti^{4+} ions of the relaxed $Ti_5O_{14}^{10-}$ layer are present in *Figure 9.42b*, which shows that the bottom flat band is largely associated with the Ti^{3+} ions, and the bottom dispersive band with both Ti^{3+} and Ti^{4+} ions.

With the unoccupied band levels lying between e_f and $e_f + \Delta$, the $\rho(r_0, e_f)$ plot can be calculated as a function of the tip-sample distance r_0. The $\rho(r_0, e_f)$ plot calculated for r_0 = 3 Å shows a bright spot centered at each oxygen vacancy site (*Figures 9.41a*). This is in good agreement with experiment and therefore supports Tanaka et al.'s interpretation that the bright spots of the STM images of $SrTiO_3$ (100) correspond to the oxygen vacancy sites of the surface.[10] As the r_0 value decreases from 3 Å, the bright spot splits into two (*Figure 9.41c* for r_0 = 2 Å, and *Figure 9.41b* for r_0 = 1 Å). All these findings reflect the fact that, in the relaxed $Ti_5O_{14}^{10-}$ layer, the band levels lying between e_f and $e_f + \Delta$ have contributions from the hybrid orbitals of the two Ti^{3+} sites flanking each oxygen vacancy.[10]

References

1. Magonov, S. N.; Whangbo, M.-H. *Surface Analysis with STM and AFM*, VCH, Weinheim, **1996**.
2. Tersoff, J.; Hamman, D. R. *Phys. Rev. B*, **1985**, 31, 85.
3. Hamers, R. J. in *Scanning Tunneling Microscopy and Spectroscopy: Theory, Techniques and Applications*, D. A. Bonnell (Ed.), VCH Publishers, New York, **1993**, Ch. 4.
4. Magonov, S. N.; Whangbo, M.-H. *Adv. Mater.*, **1994**, 6, 355.
5. (a) Tománek, D., Louie, S. G., Mamin, H. J., Abraham, D. W., Thompson, R. E., Granz, E., Clarke, J. *Phys. Rev. B*, **1987**, 35, 7790.
   (b) Tománek, D., Louie, S. G. *Phys. Rev. B*, **1988**, 37, 8327.
6. Whangbo, M.-H., Liang, W., Ren, J., Magonov, S. N., Wawkuschaewski, A. *J. Phys. Chem.*, **1994**, 98, 7602.
7. Magonov, S. N., Zönnchen, P., Roten, H., Cantow, H.-J., Thiele, G., Ren, J., Whangbo, M.-H. *J. Am. Chem. Soc.*, **1993**, 115 2495.
8. Seo, D.-K., Perdue, K., Ren, J., Whangbo, M.-H. *Surf. Sci.*, **1997**, 370 245.
9. (a) Henrich, V. E., Dresselhaus, G., Zeiger, H. J. *Phys. Rev. B*, **1978**, 17 4908.
   (b) Cord, B., Courths, R., *Surf. Sci.*, **1985**, 162 34.
10. (a) Tanaka, H., Matsumoto, T., Kawai, T., Kawai, S. *Jpn. J. Appl. Phys.*, **1993,** 32 1405.
    (b) Tanaka, H., Matsumoto, T., Kawai, T., Kawai, S. *Surf. Sic.*, **1994,** 318 29.
11. (a) Whangbo, M.-H., in *Crystal Chemistry and Properties of Materials with Quasi-One Dimensional Structures*; Rouxel, J., ed.; Reidel, Dordrecht; 1986, p. 27.
    (b) Wheeler, R. A.; Whangbo, M.-H.; Hughbanks, T.; Hoffmann, R.; Burdett, J. K.; Albright, T. A., *J. Am. Chem. Soc*. **1986**, *108* 2222.